ACS Catalysis

Research Article

Cite This: ACS Catal. 2019, 9, 10409−10417

pubs.acs.org/acscatalysis

Surface Lewis Acidity of Periphery Oxide Species as a General Kinetic Descriptor for CO_2 Hydrogenation to Methanol on Supported Copper Nanoparticles

Jonglack Kim,[†] Bidyut B. Sarma,[†] Eva Andrés,[†] Norbert Pfänder,[‡] Patricia Concepción,[§] and Gonzalo Prieto*[,†,§]

[†]Max-Planck-Institut für Kohlenforschung, Kaiser-Wilhelm-Platz 1, 45470 Mülheim an der Ruhr, Germany

[‡]Max-Planck-Institut für Chemische Energiekonversion, Stiftstraße 34-36, 45470 Mülheim an der Ruhr, Germany

[§]ITQ Instituto de Tecnología Química, Universitat Politècnica de València-Consejo Superior de Investigaciones Científicas (UPV-CSIC), Avenida de los Naranjos s/n, 46022 Valencia, Spain

Supporting Information

ABSTRACT: Oxide-supported copper nanoparticles exhibit promising properties as catalysts for the selective hydrogenation of CO_2 to methanol. Both reaction rate and selectivity depend conspicuously on the nature of the oxide support/promoter at the metal periphery. However, a major challenge is the achievement of a quantitative description of such metal/oxide promotion effects, which is an essential step toward a rational catalyst design. We investigate structure−performance relationships with a series of model catalysts consisting of Cu nanoparticles dispersed on a mesoporous γ-Al_2O_3 carrier overlaid with different transition metal oxides spanning a broad range of Lewis acidity (YO_x, ScO_x, ZrO_x, TaO_x). Remarkably, the apparent activation energy (E_a) for methanol formation is found to downscale linearly with the relative Lewis acidity of coordinatively unsaturated metal surface sites (*cus*) exposed on the oxide support, making this single physicochemical parameter a suitable reactivity descriptor in the whole study space. In correspondence with this performance trend, in situ Fourier transform infrared spectroscopy reveals that both the ionic character and the relative reactivity of bidentate formate species, developed on the catalyst surface under reaction conditions, vary systematically with the surface Lewis acidity of the oxide support. These findings support the involvement of oxide-adsorbed bidentate formate species as reaction intermediates and point to the relative electron-accepting character of the Lewis *cus* on the oxide surface as the factor determining the stability of these intermediates and the overall energy barrier for the reaction. Our results contribute a unifying and quantitative description for support effects in CO_2 hydrogenation to methanol on oxide-supported copper nanoparticles and provide a blueprint for a predictive description of metal-oxide promotion effects, which are ubiquitous in heterogeneous catalysis.

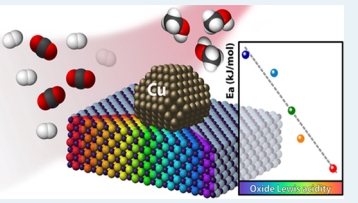

KEYWORDS: *copper catalysts, CO_2 recycling, support effects, interfacial catalysis, structure−performance relations, in situ FTIR*

INTRODUCTION

The past decade has witnessed a surge in the development of catalysts and processes for the chemical recycling of CO_2 into platform chemicals, which is regarded as a means to reduce net anthropogenic CO_2 emissions and turn waste carbon dioxide into a valuable feedstock for the chemical industry. Under certain scenarios, including the availability of cost-effective renewable hydrogen, CO_2 hydrogenation into methanol represents a sensible route to CO_2 recycling as well as to chemically store hydrogen into a versatile liquid energy carrier.[1−4]

Copper is the most attractive metal for the selective hydrogenation of CO_2 to methanol.[5−8] While the reaction has been shown to suffer from relatively high energy barriers on neat copper surfaces, which limit both reaction rates and selectivity to methanol, interfacing copper with more oxophilic oxide (or oxocarbide) species is known to result in remarkably enhanced methanol production rates.[9−12] Moreover, not only the extension of the metal-oxide boundary but also the nature of the oxide has been shown to play a decisive role for reactivity. Graciani et al.[13] showed that the deposition of patches of ZnO or CeO_2 on Cu(111) substrates led to remarkable but not equivalent increments in the reaction rate accompanied by a decline in the apparent activation energy (E_a), compared to those registered on the neat metal surface. Studt et al.[14] observed that direct contact of Cu nanocrystals with ZnO led to superior reaction rates to catalysts displaying Cu-MgO interfaces. Larmier et al.[12] reported that Cu nanoparticles deposited on ZrO_2 display notably higher reaction rates and selectivity to methanol than SiO_2-supported counterparts. Moreover, the incorporation of a variety of oxide species including ZnO_x, GaO_x, AlO_x,[15] ZrO_x,[16] or TiO_x[17] on

Received: June 10, 2019
Revised: October 2, 2019
Published: October 8, 2019

the SiO_2 surface, that is, in close proximity to the copper nanocrystals, was shown to enhance methanol formation rates to variable extents, which depended markedly on the nature of the oxide promoter.

This remarkable variability of the catalytic performance as a function of the nature of the oxide at the periphery of the metal nanoparticles makes the Cu-catalyzed CO_2 hydrogenation a paragon of the so-called metal-oxide promotion effects by which the direct contact of metal and oxide species modifies profoundly the catalytic performance of the individual components. Such promotion effects have been associated with the creation of new types of active sites at the metal-oxide boundary, electronic and morphological modifications on the metal via charge transfer or surface decoration phenomena, or the integration of various functionalities obeying different scaling relations for a common reaction intermediate within surface transport distances.[18,19] The ability to fundamentally understand these phenomena and, on this basis, engineer the structure, density, and intrinsic performance of active sites at metal-oxide interfaces holds promise for a deeper comprehension of existing catalytic systems, as well as a more rational design of innovative catalysts and processes. A genuine challenge toward this goal, however, is the identification of experimentally accessible physicochemical parameters that can help provide a quantitative, ideally universal, and predictive description of metal/oxide promotion effects.

Making use of a set of high-surface-area model catalysts where copper nanoparticles have been interfaced with a variety of transition metal oxides, the current study shows that a single experimentally quantifiable physicochemical parameter, that is, the Lewis acidity of coordinatively unsaturated metal centers exposed on the surfaces of those oxide species at the periphery of the metal nanoparticles, determines the overall energy barrier for the reaction in a broad study space. In situ and temperature-resolved FTIR studies suggest that the destabilization of bidentate formate reaction intermediates on oxide surface centers of increasingly higher electron-accepting character provides an energetically more favorable reaction pathway toward methanol formation.

RESULTS AND DISCUSSION

Catalyst Design, Synthesis, and Characterization. Our study relies on a battery of model oxide-supported catalysts designed to display similar textural properties and copper dispersion, albeit screening a very wide range of surface Lewis acidity.[20] Figure 1 summarizes conceptually the design of these catalysts. First, an array of oxide support materials was synthesized by decorating a common mesoporous γ-Al_2O_3 carrier with monolayer amounts (ca. 4.5 M_{at} nm^{-2}) of different transition metal oxides (MO_x, where M = Ta, Zr, Sc, and Y). The materials were denoted as $MO_x@Al_2O_3$. A series of MO_x oxides have been selected on the basis of their broadly different Lewis acid properties and limited reducibility under standard catalyst activation and usage conditions for CO_2 hydrogenation.

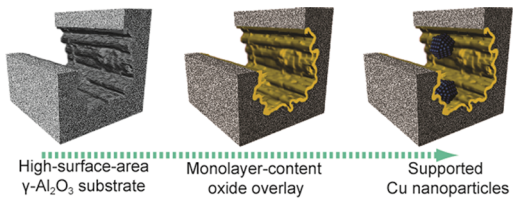

Figure 1. Schematic representation of the synthesis of Cu/MO_x@Al_2O_3 model catalysts.

For the oxide-overlaid support materials, X-ray diffraction could not detect three-dimensional oxide crystallites (Figure S1). The series of materials, including the pristine γ-Al_2O_3 substrate, displayed type-IV N_2-physisorption isotherms characteristic of mesoporous materials (Figure S2), with similar Al_2O_3-normalized specific surface areas ($277 \pm 21\ m^2\ g_{Al_2O_3}^{-1}$) and mesopore volumes ($0.71 \pm 0.06\ cm^3\ g_{Al_2O_3}^{-1}$), which discarded any significant pore blockage upon oxide incorporation (Table S1). Moreover, the average mesopore diameter decreased from 11.5 nm for the pristine γ-Al_2O_3 substrate to 9.1 ± 0.7 nm for the series of $MO_x@Al_2O_3$ materials. This ~2 nm reduction in mesopore diameter agrees reasonably well with that expected upon deposition of a monolayer of the MO_x species on the alumina surface. Jointly, these results indicate the deposition of the MO_x oxides as an amorphous (2D) overlay on the surface of the γ-Al_2O_3 substrate.

Despite their uniformity in textural features, the introduction of the oxide overlays resulted in materials differing vastly in terms of Lewis acid/base character. Oxide Lewis acidity stems from the exposure of coordinatively unsaturated metal M^{y+} sites (*cus*) on their outer surface. For the series of $MO_x@Al_2O_3$ support oxides, the surface Lewis acidity was quantitatively assessed by UV−vis spectroscopy coupled to 1,2-dihydroxyanthraquinone (alizarin) as a surface probe molecule. When adsorbed on oxide surfaces, the photon energy required to trigger the lowest intramolecular charge transfer (IMCT) from the catechol subunit to the polycyclic system, hereafter denoted as η, has been reported to be an excellent descriptor of the relative electron-accepting character of those *cus* to which the probe molecule binds (Figure 2a).[21,22] The application of this technique to determine the surface Lewis acidity of the alumina-supported $MO_x@Al_2O_3$ oxides and their corresponding unsupported (bulk) counterparts showed that oxide deposition as an overlay on the γ-Al_2O_3 surface modifies the Lewis acidity of the surface-exposed *cus* compared to the case of the crystalline bulk oxides, likely due to interactions with the γ-Al_2O_3 carrier and the lack of long-range crystalline order in the former (Figure S3). Nevertheless, as shown in Figure 2b, the acidity ranking established for the series of oxide overlays on the basis of this spectroscopic parameter remained aligned with the relative theoretical Lewis acidities of the corresponding bulk-type oxides. Therefore, the series of $MO_x@Al_2O_3$ support materials provide a unique platform of high-surface-area materials that unite essentially identical textural properties with a broad range of surface Lewis acid−base character.

Copper was incorporated at different surface contents (1.5−4.5 Cu_{at} nm^{-2}) on the series of the $MO_x@Al_2O_3$ support materials by incipient wetness impregnation. Experimental conditions for the thermal decomposition of the copper nitrate precursor were carefully adjusted to prevent its hydrolysis and achieve an effective dehydration at mild temperatures (<373 K), which results in an effective copper oxide dispersion on the surface of the support after calcination.[25,26] H_2-TPR experiments (Figure S4) showed copper reduction features to peak in a temperature window of 425−510 K. Hence, a treatment at 523 K under a flow of 20% H_2/N_2 was selected to reductively activate the catalysts prior to catalysis. After in situ reduction,

DOI: 10.1021/acscatal.9b02412
ACS Catal. 2019, 9, 10409−10417

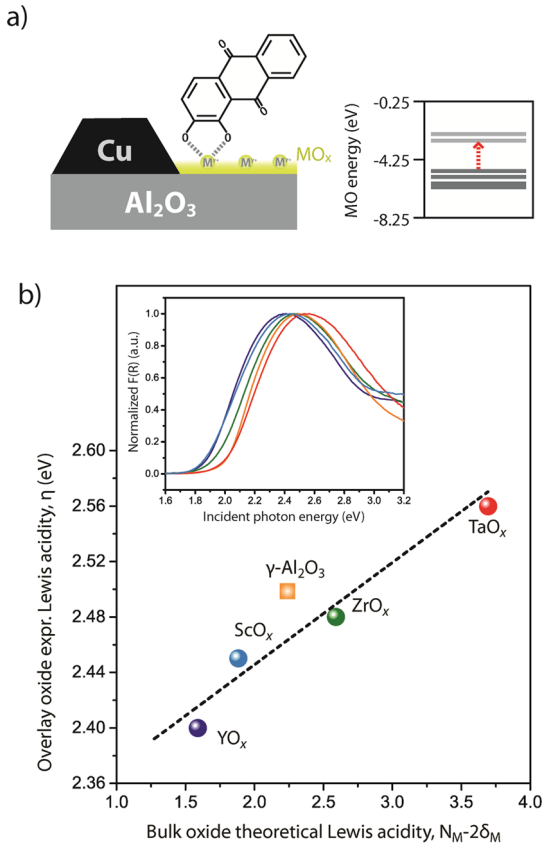

Figure 2. (a) Schematic representation of the binding of alizarin (1,2-dihydroxyanthraquinone) on coordinatively unsaturated metal sites (*cus*) exposed on the surface of the MO_x oxide overlays, together with the computed molecular orbital diagram, showing the IMCT electronic transition between the HOMO and the LUMO for the adsorbed molecule. (b) Comparison between the surface Lewis acidity determined for overlay MO_x oxides supported on γ-Al_2O_3 with the theoretical Lewis acidity of the corresponding bulk oxides determined as N_M-$2\delta_M$ where N_M represents the formal oxidation state and δ_M is Sanderson's partial charge of the cations in the bulk oxides, that is, Y_2O_3, Sc_2O_3, ZrO_2, and Ta_2O_5.[21] The inset shows the region of the UV–vis spectra where the IMCT band of the alizarin probe molecule is detected after adsorption on the different oxide supports. The data point for the uncoated γ-Al_2O_3 carrier (square symbol) has also been included in the plot. The dotted line is a guide to the eye.

X-ray photoemission spectroscopy (XPS) showed a Cu2p binding energy of 932 ± 0.4 eV, alongside a $CuL_3M_{4,5}M_{4,5}$ Auger kinetic energy of ~919 eV, suggesting full reduction to Cu^0 regardless of the nature of the oxide support. Regarding the MO_x species, binding energies corresponding to Y(III), Sc(III), Zr(IV), and Ta(V) were registered for the as-synthesized materials. No noticeable changes in the oxidation state for the M elements could be ascertained upon catalyst reduction (Figure S5). Only in the case of TaO_x could a minor (<15%) contribution from a surface Ta sub-oxide be detected after the reduction treatment. Even though the creation of surface oxygen vacancies on the oxide species cannot be excluded, these observations confirmed the relatively low reducibility of the overlay oxides selected for this study.

Copper dispersion in the series of Cu/MO_x@Al_2O_3 catalysts was studied by means of C_s-HAADF-STEM microscopy coupled to EDX spectroscopy after reduction. EDX compositional maps confirmed a remarkably uniform spatial distribution for both MO_x overlay oxides and copper at both the meso- and nanoscales (Figure S6). However, the significant Z-contrast contributed by the MO_x@Al_2O_3 oxide supports made a direct assessment of Cu nanoparticle size from STEM micrographs not reliable in the entire series of catalysts. Hence, in order to complement the local microscopy analysis and determine the overall Cu dispersion on a quantitative basis, XPS results for the in situ reduced catalysts were analyzed using the Kerkhof–Moulijn model[23] for metal crystallites supported on high-surface-area carriers, modified to account for a monolayer-thick overlay of the corresponding MO_x species on the Al_2O_3 support. The results are summarized in Figure 3. Average Cu nanoparticles sizes in the range of 4–11

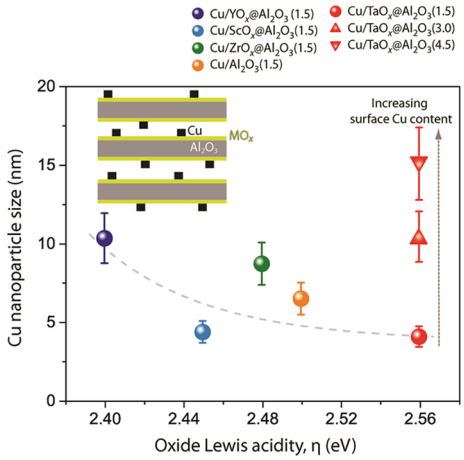

Figure 3. Average copper nanoparticle size, as quantified through the application of a modified Kerkhof–Moulijn model to the XPS spectra for Cu/MO_x@Al_2O_3 catalysts, with a surface copper content of 1.5 Cu nm^{-2} (●), 3.0 Cu nm^{-2} (▲), and 4.5 Cu nm^{-2} (▼), after reduction in hydrogen, as a function of the surface Lewis acidity of the oxide support, described with the spectroscopic parameter η. The inset shows a simplified scheme of the slab-based geometrical model applied to quantify XPS results. Error bars for the average Cu nanoparticle size correspond to the accuracy reported for the estimation of metal particle sizes from XPS data in comparison to gas chemisorption methods (ca. 15% of the average for metal NPs in the size range of 4–10 nm).[23,24] Error bars along the *x* axis are smaller than the symbols in all cases.

nm were determined for the series of catalysts synthesized with a surface copper content of 1.5 Cu nm^{-2}. The largest average size was observed for Cu nanoparticles supported on YO_x@Al_2O_3. This might be ascribed to a partial hydrolysis and agglomeration of the copper nitrate precursor during impregnation and drying, which might be promoted by the basic character of the oxide.[27] Nevertheless, similar average Cu nanoparticle sizes could be obtained on the most Lewis acidic TaO_x@Al_2O_3 carrier by increasing the surface copper content (Figure 3), as required to fully disentangle the effects of Cu nanoparticle size and oxide surface Lewis acidity on catalysis with this set of materials.

Catalysis and Structure–Performance Relationships. The CO_2 hydrogenation activity of the Cu/MO_x@Al_2O_3 catalysts was evaluated in a slurry reactor under strictly isothermal conditions. In all cases, the overall CO_2 conversion was kept differential (<5%) in order to minimize product inhibition effects on the reaction rates. For all catalysts, copper-specific initial methanol formation rates were determined to be in the range of 7.3–627.5 μmol g_{Cu}^{-1} min^{-1} in the temperature

DOI: 10.1021/acscatal.9b02412
ACS Catal. 2019, 9, 10409–10417

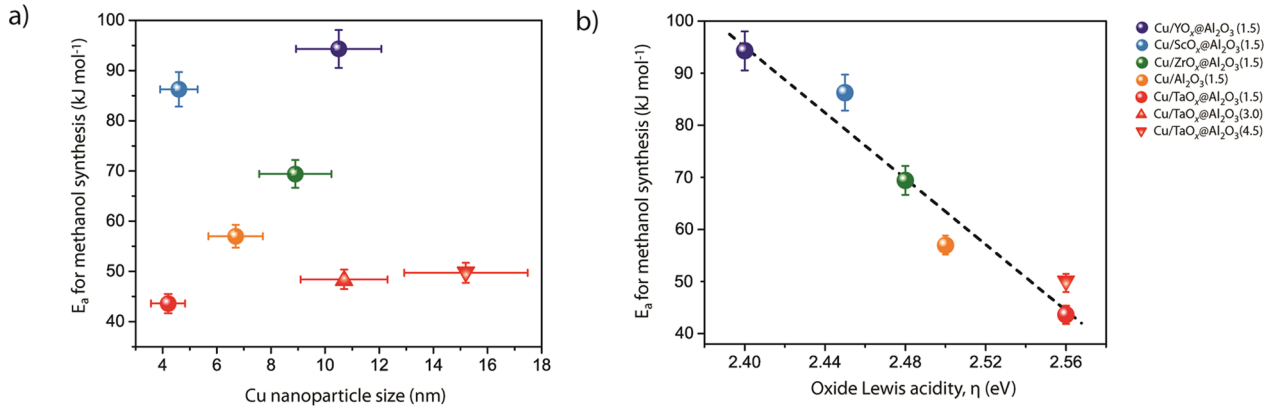

Figure 4. Dependence of the apparent activation energy for methanol synthesis with (a) the average Cu nanoparticle size and (b) the Lewis acidity of *cus* exposed on the surface of the oxide overlay interfaced with Cu nanoparticles, as described with the spectroscopic parameter η, for the series of Cu/MO$_x$@Al$_2$O$_3$ catalysts with surface copper contents of 1.5 Cu nm^{-2} (●), 3.0 Cu nm^{-2} (▲), and 4.5 Cu nm^{-2} (▼). Reaction conditions: H$_2$/CO$_2$ = 3.0, T = 433−493 K, P = 63 bar, CO$_2$ conversion < 5%. Error bars for E_a correspond to the standard error as determined from three independent tests with selected catalysts. Error bars for the average Cu nanoparticle size correspond to the accuracy reported for the estimation of metal particle sizes from XPS data in comparison to gas chemisorption methods (ca. 15% of the average for metal NPs in the size range of 4−10 nm).[23,24] Error bars for η are smaller than the symbol. The dotted line is a guide to the eye.

range of 433−493 K (Table S2). The selectivity to methanol decreased from 72−87% at 433 K to 49−56% at 493 K. Carbon monoxide, produced via the reverse water−gas shift (rWGS) reaction, was the other major carbon-based product.

The methanol formation rate is not a suitable kinetic parameter to establish structure−activity relations, as the number of surface active sites might vary for different catalysts. On the other hand, a reliable quantification of active sites and thus their intrinsic reactivity (turnover frequency, TOF) is challenging, if at all possible, for reactions requiring the concerted involvement of metallic and oxide species. On the basis of these considerations, catalytic tests were performed at preset temperatures in the range of 433−493 K and the temperature dependence of the initial methanol formation rate (Figure S7) was used to determine the apparent methanol formation activation energy (E_a). This parameter has been herein used as a kinetic descriptor, intrinsically independent of the number of active sites taking part in the reaction.

As shown in Figure 4a, no correlation exists between E_a and the Cu nanoparticle size. However, as revealed in Figure 4b, a clear linear correlation, encompassing the entire series of Cu/MO$_x$@Al$_2$O$_3$ catalysts, emerges when E_a is plotted as a function of the η spectroscopic parameter. Minor, albeit statistically significant differences in E_a were observed between Cu/TaO$_x$@Al$_2$O$_3$ with different metal contents (1.5 vs 3.0-4.5 Cu nm^{-2}) and average Cu nanoparticle sizes. The foundation of this small difference is not clear at this point, and it might be associated with changes in not only the extent but also the structure of the copper-oxide periphery with copper dispersion. The differences are, however, very modest if the variation of E_a over the entire study space is considered. Moreover, the excellent correlation observed using η as the Lewis acidity descriptor for Cu/TaO$_x$@Al$_2$O$_3$ catalysts is a strong indication that, if persistent under catalysis, the minor population of partially reduced tantalum centers, shown by XPS after reduction activation, does not affect the overall reaction kinetics to any significant extent.

These findings clearly reveal that it is the Lewis acidity of the *cus* on the surface of the oxide support, rather than the copper content or dispersion, that determines the overall energy barrier for methanol formation via CO$_2$ hydrogenation. Moreover, they furnish evidence that *cus* centers on the surface of the oxide support intervene in the catalytic turnover, for example, determining the relative reactivity of a key intermediate species in a kinetically relevant reaction step. Remarkably, an analysis of experimentally determined (apparent) activation energies reported in various literature studies underpins our finding (Figure S8). Interfacing Cu nanoparticles with oxides bearing surface *cus* of increasing Lewis acid character leads to a systematic reduction of the overall energetic barrier for methanol formation. A similar analysis based on the initial CO formation rates showed also E_a to downscale with increasing η for the series of Cu/MO$_x$@Al$_2$O$_3$ catalysts (Figure S9). Even though the dependence is notably less marked in this case than for methanol synthesis, the results suggest that the relative electron-accepting character of the *cus* sites on the peripheral oxide is also a determinant for a kinetically relevant reaction step/s of the rWGS reaction.

The mechanism of the methanol synthesis via CO$_2$ hydrogenation on copper catalysts has been the matter of significant research efforts over the last years. Two major mechanistic proposals have been put forth. On the one hand, a sequential transformation involving first the rWGS reaction via carboxylate (OCOH) intermediates followed by CO hydrogenation to methanol via methoxy (H$_3$CO) species has been considered to be energetically feasible and, even favorable, in light of quantum mechanical calculations.[11,13] Alternatively, a direct pathway has been proposed according to which CO$_2$ is first hydrogenated to formate species (HCOO$^-$) in a reaction step, which is energetically very favorable on both neat and oxide-interfaced copper surfaces.[12] Formate species are subsequently hydrogenated to methoxy species (H$_3$CO), with the concomitant release of a hydroxyl (OH) group and ultimately to methanol.[14,28] Particularly when Cu is interfaced with an oxide support/promoter, much experimental and theoretical evidence gives credence to the latter mechanistic proposal.[12,14,16,28]

Even though the actual operating mechanism remains debated, the literature richly demonstrates that the oxide catalyst component plays a pivotal role for the ultimate performance. This marked metal-oxide promotion has been ascribed to oxide surfaces being involved in the optimization of

DOI: 10.1021/acscatal.9b02412
ACS Catal. 2019, 9, 10409−10417

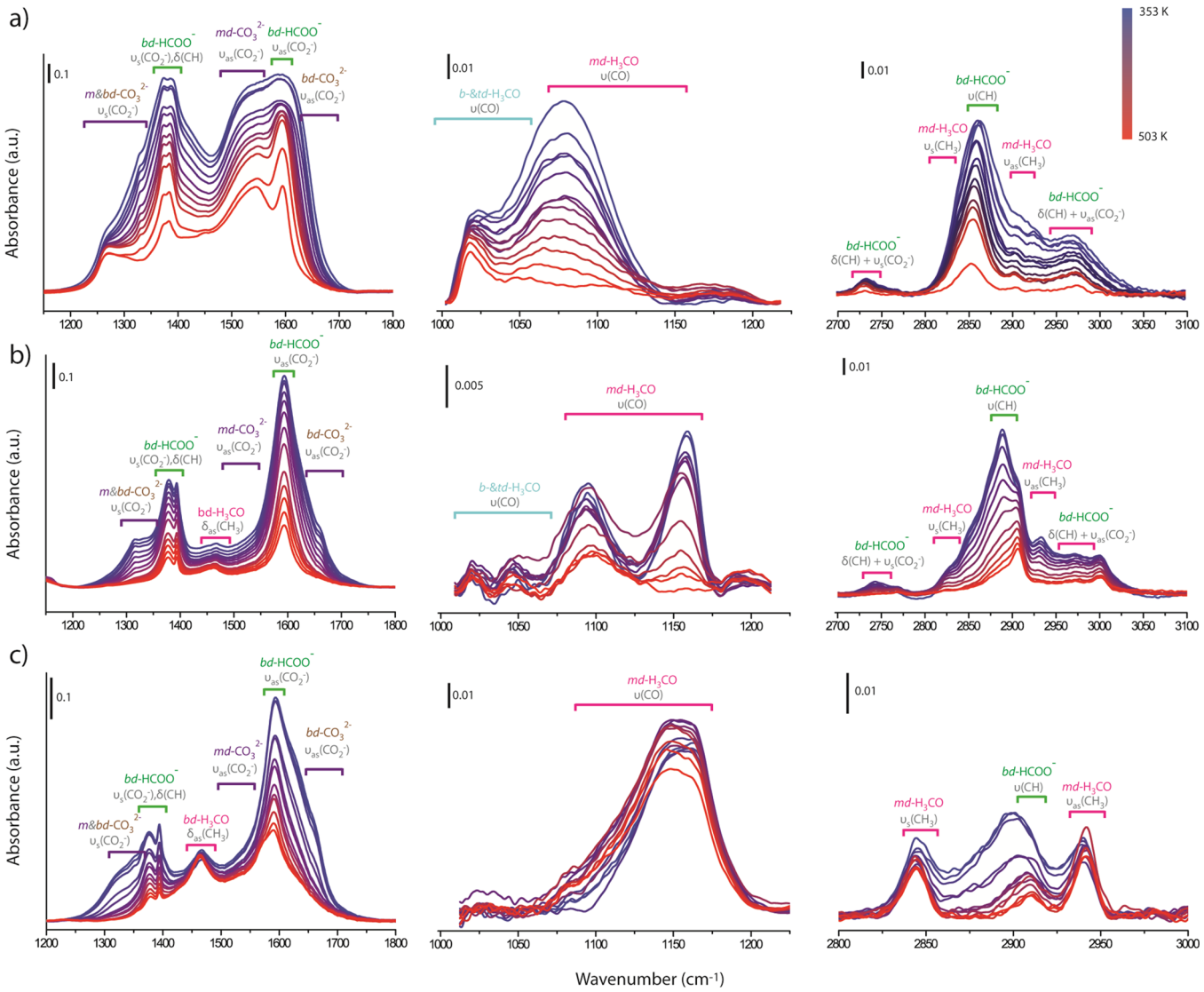

Figure 5. Temperature-resolved Fourier transform infrared (FTIR) spectra in the spectral regions characteristic for carbonitic/carboxylic OCO stretching (left panels), alkoxidic CO stretching (center panels), and CH stretching (right panels) vibrations under H_2 flow: (a) Cu/YO_x@Al_2O_3; (b) Cu/ZrO_x@Al_2O_3; (c) Cu/TaO_x@Al_2O_3 catalysts exposed to CO_2 hydrogenation conditions (T = 463 K, P = 1.02 bar, H_2/CO_2 = 3) for 2 h. In the plots, temperature is stepwise increased (blue to red spectra) with steps of 20 K from 353−413 K and 10 K thereafter until 503 K. Band nomenclature: *md*: monodentate, *bd*: bidentate, *td*: tridentate.

the binding energies—and therefore the adjustment of the reactivity—for key reaction intermediates.[11] Recent experimental and computational work from Larmier et al. has invoked the involvement of *cus* Zr^{4+} sites at the metal/oxide periphery for the development of active sites for methanol formation on Cu-ZrO_2 catalysts and proposed formate species adsorbed on these Lewis centers at the metal-oxide boundary as key reaction intermediates.[12] Additional work from the same group evidenced that Cu nanoparticles supported on a covalent, OH-terminated oxide like SiO_2, which are poorly active and methanol-selective catalysts, might be turned into efficient catalysts when the periphery of the Cu nanoparticles is populated with isolated Zr^{4+}[16] or Ti^{4+}[17] Lewis centers via surface grafting. Remarkably, our results indicate that it is the relative Lewis acidity of such *cus* centers on the oxide surface that determines the overall energy barrier for the reaction.

In Situ FTIR Spectroscopy. In situ Fourier transform infrared spectroscopy (FTIR) experiments were conducted as a means to gain molecular-level insight into the different reactivities exhibited by Cu nanoparticles supported on different oxides. The nature and relative stability of carbonaceous species, which exist on the catalyst surface under reaction conditions, were simultaneously investigated. Selected catalysts, representative of the entire range of surface Lewis acidity inspected, were first reduced in situ and then exposed to CO_2 hydrogenation conditions at 463 K for 2 h in the spectroscopic cell in order to achieve catalysis-relevant coverages of surface species. Afterward, the stability of those carbon species, which developed on the catalyst surface under reaction conditions, was assessed in a hydrogen atmosphere by FTIR-monitored temperature-programmed hydrogenation (TPH-FTIR) experiments. Figure 5 shows the temperature-resolved spectra collected for Cu/YO_x@Al_2O_3, Cu/ZrO_x@Al_2O_3, and Cu/TaO_x@Al_2O_3 catalysts in the relevant spectral regions characteristic for carbonitic/carboxylic OCO stretching (1200−1800 cm^{-1}), alkoxidic CO stretching (1000−1200 cm^{-1}), and CH stretching (2700−3000 cm^{-1}) vibrations, respectively.

DOI: 10.1021/acscatal.9b02412
ACS Catal. 2019, 9, 10409−10417

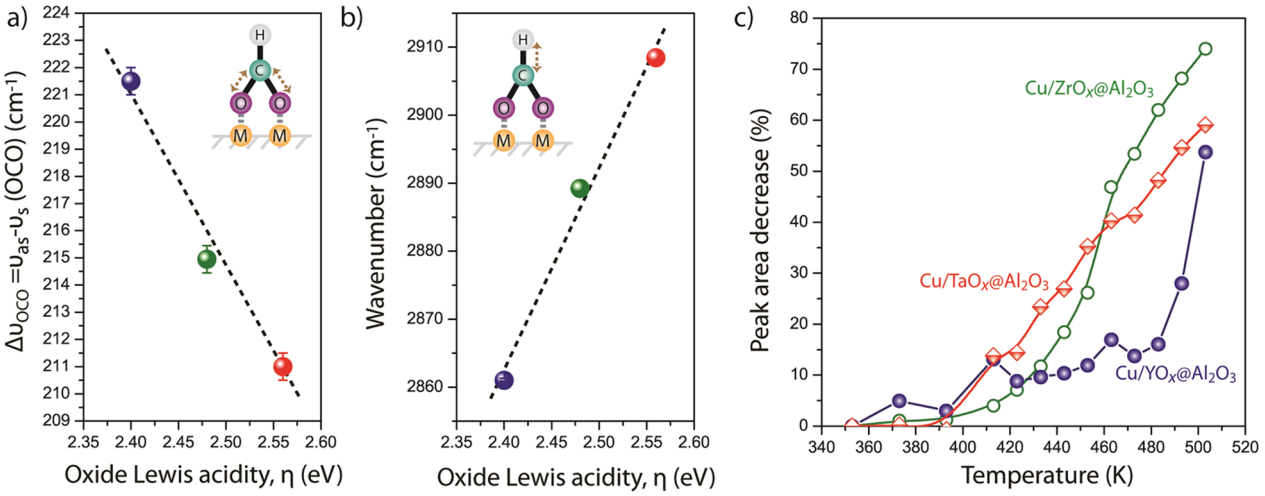

Figure 6. (a) Band split between the symmetric and asymmetric υ(OCO) stretching modes and (b) frequency for the υ(CH) stretching mode observed for bidentate surface formate species developed under CO_2 hydrogenation conditions on the surface of Cu/YO_x@Al_2O_3 (blue), Cu/ZrO_x@Al_2O_3 (green), and Cu/TaO_x@Al_2O_3 (red) catalysts as a function of the relative Lewis acidity of *cus* on the MO_x@Al_2O_3 oxide support, as described with the spectroscopic parameter η. (c) Temperature-resolved evolution of the intensity of the OCO asymmetric stretching FTIR band for bidentate surface formate species under H_2 flow for Cu/YO_x@Al_2O_3 (blue), Cu/ZrO_x@Al_2O_3 (green), and Cu/TaO_x@Al_2O_3 (red) catalysts.

After exposure to CO_2 hydrogenation conditions, the spectrum for Cu/YO_x@Al_2O_3 in the υ(OCO) region corresponds to the convolution of various contributions, reflecting a wide diversity of surface species (Figure 5a). Bidentate formate species ($HCOO^-$) can be identified by an intense absorption band at ~1596 cm^{-1} ($\upsilon_{as}(CO_2^-)$) alongside a split band at ~1380 cm^{-1} (δ(CH) and $\upsilon_s(CO_2^-)$).[11,29,30] The detection of this species is confirmed by the observation of a prominent band at 2861 cm^{-1}, which is ascribed to the υ(CH) vibration mode. In addition, a variety of carbonate (CO_3^{2-}) species, including various surface binding configurations, is inferred from the broad contributions in the regions of 1450−1550 and 1620−1670 cm^{-1}, ascribed to the asymmetric υ_{as}(OCO) mode of mono- and bidentate carbonates (CO_3^{2-}), respectively, and the region of 1280−1390 cm^{-1}, corresponding to symmetric υ_s(OCO) vibrations.[29] These species likely form via insertion of CO_2 into basic O^{2-} groups on the surface of the YO_x overlay oxide. Copper-bonded formate species ($\upsilon_{as}(CO_2^-)$ at 1530−1600 cm^{-1}, $\upsilon_s(CO_2^-)$ at 1315−1360 cm^{-1})[31−33] and carboxylate (OCO^-) species ($\upsilon_{as}(CO_2^-)$ at 1550−1570 cm^{-1}, $\upsilon_s(CO_2^-)$ at 1350−1370 cm^{-1})[34] might also exist on the catalyst surface. No formation of surface hydrogen carbonates (HCO_3^-) could be ascertained, owing to the absence of absorption bands in the regions of 3500−3700 and 1200−1250 cm^{-1}, which could be ascribed to the υ(OH) and δ(OH) vibrations, respectively, for these species.

A notably lower surface carbonate coverage is inferred from the analysis of the υ(OCO) spectral region for catalysts supported on oxides of progressively higher surface Lewis acidity, that is, Cu/ZrO_x@Al_2O_3 and Cu/TaO_x@Al_2O_3 (Figure 5b,c, respectively). In these cases, the spectra are clearly dominated by bands assigned to bidentate formate species. These groups show an intense band at 1593 cm^{-1} ($\upsilon_{as}(CO_2^-)$), with a less intense and clearly split doublet at 1378 and 1393 cm^{-1} (δ(CH) and $\upsilon_s(CO_2^-)$) for Cu/ZrO_x@Al_2O_3. Similarly, a major signal peaking at ~1588 cm^{-1} ($\upsilon_{as}(CO_2^-)$), with a weaker doublet at 1377 and 1394 cm^{-1} (δ(CH) and $\upsilon_s(CO_2^-)$) is observed in the case of Cu/TaO_x@Al_2O_3. Deconvolution of the spectra (Figure S10) enabled the analysis of the temperature-resolved evolution of individual signals, as well as the establishment of correspondence between different IR active modes arising from a single surface species. This was particularly useful in the region of CH stretching modes (2700−3000 cm^{-1}) where the registration of combination bands and Fermi resonances thereof with fundamental modes makes spectrum interpretation more difficult. In this spectral region, bidentate formate groups showed intense υ(CH) bands peaking at 2890 and 2909 cm^{-1} on Cu/ZrO_x@Al_2O_3 and Cu/TaO_x@Al_2O_3 catalysts, respectively.[11,35]

Interestingly, our results provide evidence that the nature of the predominant formate surface species varies systematically with the surface Lewis acidity of the oxide support, confirming that these groups bind to the *cus* on the oxide surface. Figure 6a shows the evolution of the $\Delta\upsilon_{OCO} = \upsilon_{as} - \upsilon_s$ band split for the OCO stretching modes in surface formate species as a function of the spectroscopic parameter η for the oxide support. Band splits around 215 cm^{-1} indicate bidentate surface binding configurations in all cases. More remarkably, deviations of $\Delta\upsilon_{OCO}$ with respect to the band split observed for the free formate ion in solution ($\Delta\upsilon_{OCO} = \upsilon_4 - \upsilon_2 = 234$ cm^{-1})[36] are in relation to the degree of electronic/structural distortion in the adsorbed state. As observed, $\Delta\upsilon_{OCO}$ decreases monotonically upon increasing η. For the same species, Figure 6b shows a linear blue-shift in the υ(CH) fundamental mode with increasing η. This vibrational mode is particularly sensitive to changes in the ionicity degree of formate species.[37] Albeit differences in the O−C−O bond angle cannot be discarded, these trends may be rationalized as a systematic modification of the electronic properties of surface formate species as a function of the relative electron-accepting character of those *cus* Lewis centers on the surface of the oxide support they bind to. Centers of increasing electron-withdrawing character on the surface of increasingly stronger Lewis acidic oxides (from Y^{3+} on YO_x@Al_2O_3 to Ta^{5+} on TaO_x@Al_2O_3) stabilize formate species with decreasing ionic character, hence bearing a carbon atom of increasing electrophilic character.

DOI: 10.1021/acscatal.9b02412
ACS Catal. 2019, 9, 10409−10417

Inspection of the spectra in the region for υ(CO) vibrations of surface alkoxidic species (1000−1200 cm^{-1}) reveals also the presence of methoxy groups on the surface of all catalysts after exposure to CO_2 hydrogenation conditions. Particularly for catalysts of intermediate ($Cu/ZrO_x@Al_2O_3$) and high ($Cu/TaO_x@Al_2O_3$) surface Lewis acidity, vibration frequencies >1080 cm^{-1} indicate that the methoxy groups are mostly monodentate (on-top) species singly bonded to *cus* metal centers on the oxide surface.[38] These species are also characterized by $\upsilon_s(CH_3)$ and $\upsilon_{as}(CH_3)$ bands at ∼2835−2845 and 2930−2940 cm^{-1},[38] respectively, observed in the CH stretching spectral region. In the case of the most Lewis basic $Cu/YO_x@Al_2O_3$, additional υ(CO) contributions peaking in the 1016−1028 cm^{-1} range could be assigned to either methoxy species adsorbed in a multidentate configuration on the oxide support or methoxy groups bonded to the copper surface.[38−40] Their remarkable thermal stability (Figure 5a) suggests the former assignment to be more appropriate.

Previous quantum-mechanical computations have deemed both formate and methoxy groups to be the energetically most stable species along the so-called formate route mechanism for CO_2 hydrogenation on Cu-oxide catalysts.[12,14,41] This fact renders them major candidates to play the role of key reaction intermediates, that is, those involved in the rate-determining elementary step. We have analyzed the relative reactivity of different surface species by following the evolution of their FTIR fingerprint bands as a function of the temperature during TPH-FTIR experiments. On increasing the temperature, most bands progressively tapered off, indicating a decrease in the surface coverage as the corresponding adsorbates are converted. However, few signals showed only minor intensity changes, which suggests a remarkable stability of the corresponding surface species in the temperature range examined.

As shown in Figure 6c, significantly different reactivities are observed for formate species developed on the surface of different catalysts. Formate conversion, as monitored by the intensity decrease registered for the υ_{as}(OCO) band, sets in at 393−413 K for the most Lewis acidic $Cu/TaO_x@Al_2O_3$ and proceeds steadily over the entire temperature range examined. Conversely, no major changes in formate surface coverage are inferred for the most Lewis basic $Cu/YO_x@Al_2O_3$ counterpart until a rather high temperature of 473−483 K, beyond which a very steep formate conversion is observed. These behaviors are reminiscent of reactions showing comparatively low and high activation energies, respectively. The temperature-resolved formate consumption profile for $Cu/ZrO_x@Al_2O_3$, which bears an oxide overlay of intermediate Lewis acidity, shows also an intermediate behavior. It should be noted that not all formate groups, which are converted at a given temperature under pure H_2 during the TPH-FTIR experiments (transient surface coverage), would necessarily turn over under reaction conditions (pseudo-steady surface coverage) where proximity of oxide-bonded species to the copper surface might be decisive for the frequency of site renovation. Nevertheless, our results clearly enlighten differences in the relative stability of these bidentate formate species as a function of the relative acidity of the *cus* Lewis centers on the surface of the oxide at the periphery of the copper nanoparticles.

A similar TPH-FTIR analysis for surface methoxy species showed the reverse trend (Figure S11). On increasing the temperature, methoxy υ(CO) bands vanish steadily to essentially full conversion for the most Lewis basic $Cu/YO_x@Al_2O_3$. In stark contrast, these species show barely any conversion on the most Lewis acidic surface of $Cu/TaO_x@Al_2O_3$, as all their characteristic bands, that is, υ(CO) at 1145−1165 cm^{-1}, $\delta_{as}(CH_3)$ at 1465 cm^{-1}, and $\upsilon(CH_3)$ at 2844 (symmetric) and 2941 cm^{-1} (asymmetric), undergo essentially no net intensity decrease in the temperature range screened. Rather, a certain accumulation of methoxy groups is inferred at intermediate temperatures (373−473 K), which, in the absence of gas-phase CO_2, necessarily indicates their formation by hydrogenation of other surface intermediates (e.g., formates) and/or readsorption of the methanol product on the catalyst surface (Figure S11).

Overall, TPH-FTIR results show that the relative reactivity of oxide-bonded bidentate formate species under H_2 scales with the Lewis acidity of the *cus* centers on the oxide support in a parallel fashion to the overall activation energy for methanol formation. This finding suggests the involvement of these species as key reaction intermediates, in agreement with mechanistic proposals based on the formate route.[12,14] In light of this observation, alongside those differences in ionic character inferred for these species as a function of the surface oxide Lewis acidity, it is sensible to hypothesize that an increasing electronic transfer to *cus* oxide Lewis centers of increasing electron-withdrawing character contributes to the destabilization of these reaction intermediates and thus the decrease in E_a observed experimentally for methanol formation. These results are reminiscent of previous computational predictions on the hydrogenation of formate species to methoxy groups, activated by organoaluminum molecular Lewis acids.[42] As inferred from computed reaction energy profiles, the quenching of the electron density around the carbon center in formate intermediates bound to Lewis centers of increasing acidity enhances its electrophilic character and makes it more susceptible to nucleophilic attack by hydride species, as required to undergo hydrogenation into methoxy groups.[42] A similar effect might be at play at Cu-oxide interfaces on solid catalysts.

In contrast to formate groups, the relative reactivity of surface methoxy species scales inversely with the Lewis acidity of the *cus* on the oxide surface. Hence, our results suggest that these surface groups are unlikely to be involved in a kinetically relevant reaction step. On the contrary, the accumulation and persistence of these relatively basic species on oxide surface centers of marked Lewis acidic character, that is, Ta^{5+} centers on $Cu/TaO_x@Al_2O_3$, suggest that they might play a role in product site inhibition phenomena, which have been consistently observed on Cu catalysts supported on oxides of medium-to-high Lewis acidity at high reactant contact times.[12,17,28]

These results can be regarded as a guideline for the development of copper catalysts for CO_2 hydrogenation and suggest the Lewis acidity (relative electron-accepting character) of coordinatively unsaturated cationic centers exposed on the surface of the oxide support as a key catalyst design parameter. While illustrated herein for oxide-supported copper catalysts, similar studies could potentially be extended to alternative, non-oxidic support materials, such as other chalcogenides or metal carbides, which have also been explored as carriers for Cu-based CO_2 hydrogenation catalysts[10,43] and for which the ionic character and thus the acidity of surface-exposed *cus* Lewis centers might be modulated via composition.

DOI: 10.1021/acscatal.9b02412
ACS Catal. 2019, 9, 10409−10417

CONCLUSIONS

An array of model solid catalysts was synthesized by dispersing copper nanoparticles on a high-surface-area γ-Al_2O_3 carrier, previously overcoated with monolayer contents of various transition metal oxides (YO_x, ScO_x, ZrO_x, TaO_x). Within this set of catalysts, copper nanoparticles are interfaced with metal oxides exposing coordinatively unsaturated metal sites (*cus*) of notably different Lewis acidities, as quantified by UV−vis spectroscopy coupled to 1,2-dihydroxyanthraquinone as a surface probe. Under relevant CO_2 hydrogenation conditions, the apparent activation energy for methanol formation scaled inversely with the Lewis acidity of the *cus* sites on the oxide catalyst component. Our observation renders this single physicochemical parameter a generally valid reactivity descriptor in the whole study space and furnishes evidence for the participation of Lewis acid centers on the periphery oxide in a kinetically relevant reaction step. In situ and temperature-resolved FTIR studies revealed that both the relative ionic character and the stability of bidentate formate species, which develop on the oxide catalyst surface under reaction conditions, depend systematically on the electron-accepting character of the oxide *cus*. In correspondence to the catalytic activity trend, oxide binding centers of increasing Lewis acidity bind formate species, which display comparatively higher reactivity in the presence of hydrogen, suggesting their role as reaction intermediates. The opposite behavior was observed for surface methoxy species, which were found to be remarkably stabilized by oxide *cus* of substantial Lewis acid character, advocating against the participation of these species in a kinetically relevant reaction step. By identifying a suitable, seemingly general, and experimentally accessible physicochemical descriptor for oxide support effects, this study sets the scene for a more rational design of advanced copper catalysts for the selective hydrogenation of CO_2 to methanol and potentially other catalytic reactions where performance is dominated by metal-oxide promotion effects.

ASSOCIATED CONTENT

Supporting Information

The Supporting Information is available free of charge on the ACS Publications website at DOI: 10.1021/acscatal.9b02412.

Detailed experimental methods (with Figures EM1 and EM2) and supporting data, including X-ray diffraction patterns, N_2-physisorption, H_2-TPR, XPS, STEM-EDX, details on FTIR spectra deconvolution and catalytic data (Figures S1 to S11; Tables S1 and S2) (PDF)

AUTHOR INFORMATION

Corresponding Author

*E-mail: prieto@mpi-muelheim.mpg.de.

ORCID

Patricia Concepción: 0000-0003-2058-3103

Gonzalo Prieto: 0000-0002-0956-3040

Notes

The authors declare no competing financial interest.

ACKNOWLEDGMENTS

The authors are grateful to P. Bussian and Sasol for providing the alumina precursor. S. Ruthe and K. Jeske (MPI-KOFO) are acknowledged for assistance with chromatographic product quantification. J. M. Salas (ITQ) and J. P. Holgado (ICMS-CSIC, Spain) are acknowledged for contributions to the in situ FTIR and XPS experiments, respectively. This research received funding from the Max Planck Society, the Bundesministerium für Bildung und Forschung (project 01DG17019), the Spanish Ministry of Science, Innovation and Universities (Severo Ochoa Excellence award SEV-2016-0683), and the Generalitat Valenciana (Scientific Excellence of Junior Researchers, SEJI2018/011). B.S. acknowledges the Humboldt foundation for a postdoctoral fellowship.

REFERENCES

(1) Goeppert, A.; Czaun, M.; Jones, J.-P.; Surya Prakash, G. K.; Olah, G. A. Recycling of Carbon Dioxide to Methanol and Derived Products − Closing the Loop. *Chem. Soc. Rev.* **2014**, *43*, 7995−8048.

(2) Álvarez, A.; Bansode, A.; Urakawa, A.; Bavykina, A. V.; Wezendonk, T. A.; Makkee, M.; Gascon, J.; Kapteijn, F. Challenges in the Greener Production of Formates/Formic Acid, Methanol, and DME by Heterogeneously Catalyzed CO_2 Hydrogenation Processes. *Chem. Rev.* **2017**, *117*, 9804−9838.

(3) Prieto, G. Carbon Dioxide Hydrogenation into Higher Hydrocarbons and Oxygenates: Thermodynamic and Kinetic Bounds and Progress with Heterogeneous and Homogeneous Catalysis. *ChemSusChem* **2017**, *10*, 1056−1070.

(4) Olah, G. A. Beyond Oil and Gas: The Methanol Economy. *Angew.Chem., Int. Ed.* **2005**, *44*, 2636−2639.

(5) Bando, K. K.; Sayama, K.; Kusama, H.; Okabe, K.; Arakawa, H. In-Situ FT-IR Study on CO_2 Hydrogenation over Cu Catalysts Supported on SiO_2, Al_2O_3, and TiO_2. *Appl. Catal., A* **1997**, *165*, 391−409.

(6) Schild, C.; Wokaun, A.; Baiker, A. On the Mechanism of CO and CO_2 Hydrogenation Reactions on Zirconia-Supported Catalysts: A Diffuse Reflectance FTIR study. *J. Mol. Catal.* **1990**, *63*, 243−254.

(7) Bansode, A.; Urakawa, A. Towards Full One-Pass Conversion of Carbon Dioxide to Methanol and Methanol-Derived Products. *J. Catal.* **2014**, *309*, 66−70.

(8) Behrens, M. Heterogeneous Catalysis of CO_2 Conversion to Methanol on Copper Surfaces. *Angew.Chem., Int. Ed.* **2014**, *53*, 12022−12024.

(9) Fujitani, T.; Nakamura, I.; Uchijima, T.; Nakamura, J. The Kinetics and Mechanism of Methanol Synthesis by Hydrogenation of CO_2 over a Zn-Deposited Cu(111) Surface. *Surf. Sci.* **1997**, *383*, 285−298.

(10) Rodriguez, J. A.; Liu, P.; Stacchiola, D. J.; Senanayake, S. D.; White, M. G.; Chen, J. G. Hydrogenation of CO_2 to Methanol: Importance of Metal−Oxide and Metal−Carbide Interfaces in the Activation of CO_2. *ACS Catal.* **2015**, *5*, 6696−6706.

(11) Kattel, S.; Yan, B.; Yang, Y.; Chen, J. G.; Liu, P. Optimizing Binding Energies of Key Intermediates for CO_2 Hydrogenation to Methanol over Oxide-Supported Copper. *J. Am. Chem. Soc.* **2016**, *138*, 12440−12450.

(12) Larmier, K.; Liao, W.-C.; Tada, S.; Lam, E.; Verel, R.; Bansode, A.; Urakawa, A.; Comas-Vives, A.; Copéret, C. CO_2-to-Methanol Hydrogenation on Zirconia-Supported Copper Nanoparticles: Reaction Intermediates and the Role of the Metal-Support Interface. *Angew. Chem., Int. Ed.* **2017**, *56*, 2318−2323.

(13) Graciani, J.; Mudiyanselage, K.; Xu, F.; Baber, A. E.; Evans, J.; Senanayake, S. D.; Stacchiola, D. J.; Liu, P.; Hrbek, J.; Sanz, J. F.; Rodriguez, J. A. Highly Active Copper-Ceria and Copper-Ceria-Titania Catalysts for Methanol Synthesis from CO_2. *Science* **2014**, *345*, 546−550.

(14) Studt, F.; Behrens, M.; Kunkes, E. L.; Thomas, N.; Zander, S.; Tarasov, A.; Schumann, J.; Frei, E.; Varley, J. B.; Abild-Pedersen, F.; Nørskov, J. K.; Schlögl, R. The Mechanism of CO and CO_2 Hydrogenation to Methanol over Cu-Based Catalysts. *ChemCatChem* **2015**, *7*, 1105−1111.

(15) Burch, R.; Golunski, S. E.; Spencer, M. S. The Role of Copper and Zinc Oxide in Methanol Synthesis Catalysts. *J. Chem. Soc., Faraday Trans.* **1990**, *86*, 2683−2691.

DOI: 10.1021/acscatal.9b02412
ACS Catal. 2019, 9, 10409−10417

(16) Lam, E.; Larmier, K.; Wolf, P.; Tada, S.; Safonova, O. V.; Copéret, C. Isolated Zr Surface Sites on Silica Promote Hydrogenation of CO_2 to CH_3OH in Supported Cu Catalysts. *J. Am. Chem. Soc.* **2018**, *140*, 10530−10535.
(17) Noh, G.; Lam, E.; Alfke, J. L.; Larmier, K.; Searles, K.; Wolf, P.; Copéret, C. Selective Hydrogenation of CO_2 to CH_3OH on Supported Cu Nanoparticles Promoted by Isolated Ti^{IV} Surface Sites on SiO_2. *ChemSusChem* **2019**, *12*, 968−972.
(18) Kumar, G.; Nikolla, E.; Linic, S.; Medlin, J. W.; Janik, M. J. Multicomponent Catalysts: Limitations and Prospects. *ACS Catal.* **2018**, *8*, 3202−3208.
(19) Ro, I.; Resasco, J.; Christopher, P. Approaches for Understanding and Controlling Interfacial Effects in Oxide-Supported Metal Catalysts. *ACS Catal.* **2018**, *8*, 7368−7387.
(20) Prieto, G.; Concepción, P.; Martínez, A.; Mendoza, E. New Insights into the Role of the Electronic Properties of Oxide Promoters in Rh-Catalyzed Selective Synthesis of Oxygenates from Synthesis Gas. *J. Catal.* **2011**, *280*, 274−288.
(21) Jeong, N. C.; Lee, J. S.; Tae, E. L.; Lee, Y. J.; Yoon, K. B. Acidity Scale for Metal Oxides and Sanderson's Electronegativities of Lanthanide Elements. *Angew. Chem., Int. Ed.* **2008**, *47*, 10128−10132.
(22) Prieto, G.; De Mello, M. I. S.; Concepción, P.; Murciano, R.; Pergher, S. B. C.; Martínez, A. Cobalt-Catalyzed Fischer−Tropsch Synthesis: Chemical Nature of the Oxide Support as a Performance Descriptor. *ACS Catal.* **2015**, *5*, 3323−3335.
(23) Kerkhof, F. P. J. M.; Moulijn, J. A. Quantitative Analysis of XPS Intensities for Supported Catalysts. *J. Phys. Chem.* **1979**, *83*, 1612−1619.
(24) Di Castro, V.; Furlani, C.; Gargano, M.; Ravasio, N.; Rossi, M. XPS Study of Copper Dispersion in CuO/Al_2O_3 Catalysts. *J. Electron Spectrosc. Relat. Phenom.* **1990**, *52*, 415−422.
(25) Munnik, P.; Wolters, M.; Gabrielsson, A.; Pollington, S. D.; Headdock, G.; Bitter, J. H.; de Jongh, P. E.; de Jong, K. P. Copper Nitrate Redispersion to Arrive at Highly Active Silica-Supported Copper Catalysts. *J. Phys. Chem. C* **2011**, *115*, 14698−14706.
(26) Prieto, G.; Zečević, J.; Friedrich, H.; de Jong, K. P.; de Jongh, P. E. Towards Stable Catalysts by Controlling Collective Properties of Supported Metal Nanoparticles. *Nat. Mater.* **2013**, *12*, 34−39.
(27) Prieto, G.; Shakeri, M.; de Jong, K. P.; de Jongh, P. E. Quantitative Relationship between Support Porosity and the Stability of Pore-Confined Metal Nanoparticles Studied on $Cuzno/SiO_2$ Methanol Synthesis Catalysts. *ACS Nano* **2014**, *8*, 2522−2531.
(28) Kunkes, E. L.; Studt, F.; Abild-Pedersen, F.; Schlögl, R.; Behrens, M. Hydrogenation of CO_2 to Methanol and CO on $Cu/ZnO/Al_2O_3$: Is There a Common Intermediate or Not? *J. Catal.* **2015**, *328*, 43−48.
(29) Turek, A. M.; Wachs, I. E.; DeCanio, E. Acidic Properties of Alumina-Supported Metal Oxide Catalysts: An Infrared Spectroscopy Study. *J. Phys. Chem.* **1992**, *96*, 5000−5007.
(30) Vayssilov, G. N.; Mihaylov, M.; Petkov, P. S.; Hadjiivanov, K. I.; Neyman, K. M. Reassignment of the Vibrational Spectra of Carbonates, Formates, and Related Surface Species on Ceria: A Combined Density Functional and Infrared Spectroscopy Investigation. *J. Phys. Chem. C* **2011**, *115*, 23435−23454.
(31) Hayden, B. E.; Prince, K.; Woodruff, D. P.; Bradshaw, A. M. An IRAS Study of Formic Acid and Surface Formate Adsorbed on Cu(110). *Surf. Sci.* **1983**, *133*, 589−604.
(32) Chutia, A.; Silverwood, I. P.; Farrow, M. R.; Scanlon, D. O.; Wells, P. P.; Bowker, M.; Parker, S. F.; Catlow, C. R. A. Adsorption of Formate Species on Cu(h,k,l) Low Index Surfaces. *Surf. Sci.* **2016**, *653*, 45−54.
(33) Lin, J.; Neoh, K. G.; Teo, W. k. Thermogravimetry−Ftir Study of the Surface Formate Decomposition on Cu, CuCl, Cu_2O and CuO. Correlations between Reaction Selectivity and Structural Properties. *J. Chem. Soc., Faraday Trans.* **1994**, *90*, 355−362.
(34) Millar, G. J.; Rochester, C. H.; Waugh, K. C. Infrared Study of CO, CO_2, H_2 and H_2O Interactions on Potassium-Promoted Reduced and Oxidised Silica-Supported Copper Catalysts. *J. Chem. Soc., Faraday Trans.* **1992**, *88*, 1477−1488.
(35) Köck, E.-M.; Kogler, M.; Bielz, T.; Klötzer, B.; Penner, S. In Situ FT-IR Spectroscopic Study of CO_2 and CO Adsorption on Y_2O_3, ZrO_2, and Yttria-Stabilized ZrO_2. *J. Phys. Chem. C* **2013**, *117*, 17666−17673.
(36) Ito, K.; Bernstein, H. J. The Vibrational Spectra of the Formate, Acetate, and Oxalate Ions. *Can. J. Chem.* **1956**, *34*, 170−178.
(37) Busca, G.; Lamotte, J.; Lavalley, J. C.; Lorenzelli, V. FT-IR Study of the Adsorption and Transformation of Formaldehyde on Oxide Surfaces. *J. Am. Chem. Soc.* **1987**, *109*, 5197−5202.
(38) Wu, W.-C.; Chuang, C.-C.; Lin, J.-L. Bonding Geometry and Reactivity of Methoxy and Ethoxy Groups Adsorbed on Powdered TiO_2. *J. Phys. Chem. B* **2000**, *104*, 8719−8724.
(39) Daturi, M.; Binet, C.; Lavalley, J. C.; Blanchard, G. Surface Ftir Investigations on $Ce_xZr_{1-X}O_2$ System. *Surf. Interface Anal.* **2000**, *30*, 273−277.
(40) Silva, S. L.; Pham, T. M.; Patel, A. A.; Haq, S.; Leibsle, F. M. STM and FTIR Studies of Methoxy and Acetate on Cu(110) Surfaces Resulting from Reactions with Methyl Acetate and Preadsorbed Oxygen. *Surf. Sci.* **2000**, *452*, 79−94.
(41) Grabow, L. C.; Mavrikakis, M. Mechanism of Methanol Synthesis on Cu through CO_2 and CO Hydrogenation. *ACS Catal.* **2011**, *1*, 365−384.
(42) Roy, L.; Ghosh, B.; Paul, A. Lewis Acid Promoted Hydrogenation of CO_2 and HCOO−by Amine Boranes: Mechanistic Insight from a Computational Approach. *J. Phys. Chem. A* **2017**, *121*, 5204−5216.
(43) Vidal, A. B.; Feria, L.; Evans, J.; Takahashi, Y.; Liu, P.; Nakamura, K.; Illas, F.; Rodriguez, J. A. CO_2 Activation and Methanol Synthesis on Novel Au/TiC and Cu/TiC Catalysts. *J. Phys. Chem. Lett.* **2012**, *3*, 2275−2280.

DOI: 10.1021/acscatal.9b02412
ACS Catal. 2019, 9, 10409−10417